Supplement of Clim. Past, 22, 1559–1584, 2026
https://doi.org/10.5194/cp-22-1559-2026-supplement

Supplement of

Increased abyssal ocean density stratification across the Middle Pleistocene Transition

Nicola C. Thomas et al.

Correspondence to: Nicola C. Thomas (nct30@cam.ac.uk, nct3051@gmail.com)

Carbonate ion effect

Foraminiferal Mg/Ca ratios are increasingly used as an independent proxy for estimating seawater palaeotemperatures exploiting the temperature dependent partitioning of Mg during calcification (Elderfield et al., 2006, 2010; Greaves, 2008; Mashiotta et al., 1999; Weldeab et al., 2016), whereby higher Mg ion concentrations are incorporated into foraminiferal calcite lattice with increasing seawater temperature (Elderfield et al., 2010; Greaves, 2008; Mashiotta et al., 1999). Because Mg incorporation in biogenic calcite is biologically mediated, species-specific empirical calibrations are required to estimate past deep-water palaeotemperatures (Elderfield et al., 2006, 2010; Greaves, 2008). For some benthic species, such as the epifaunal *Cibicidoides wuellerstorfi* (Sosdian and Rosenthal, 2009) palaeotemperature calibrations may be complicated by the influence of [CO_3^{2-}] on the incorporation of Mg during calcification (Elderfield et al., 2006, 2012; Weldeab et al., 2016; Yu and Broecker, 2010; Yu and Elderfield, 2008). Notably, *Cibicidoides wuellerstorfi* exhibits weaker Mg/Ca sensitivity to temperature relative to both *Uvigerina* spp. (Elderfield et al., 2006, 2010) and *Globobulimina affinis* (Weldeab et al., 2016). These infaunal benthic foraminifera, *Uvigerina* spp. and *Globobulimina* spp., which are shallow (1–2 cm) and deep (>1–10 cm) dwelling below the sediment-bottom water interface respectively, are buffered from [CO_3^{2-}] (Elderfield et al., 2006; Stirpe et al., 2021) because they form their tests from pore waters in which $CaCO_3$ remains saturated (Birner et al., 2016; Elderfield et al., 2006, 2010; Martin and Sayles, 1996). Whereas recent evidence suggests porewater Δ[CO_3^{2-}] is spatially and temporally variable with greater potential to influence *Uvigerina* spp. Mg/Ca than originally thought (Weldeab et al., 2016), *Uvigerina* spp. do not appear to be significantly affected by deep-water changes in carbonate chemistry (Elderfield et al., 2010; Stirpe et al., 2021). Furthermore, Mg/Ca measured in *Globobulimina* spp. has a relatively high temperature sensitivity affording a robust means to estimate past deep-water temperatures (Weldeab et al., 2016).

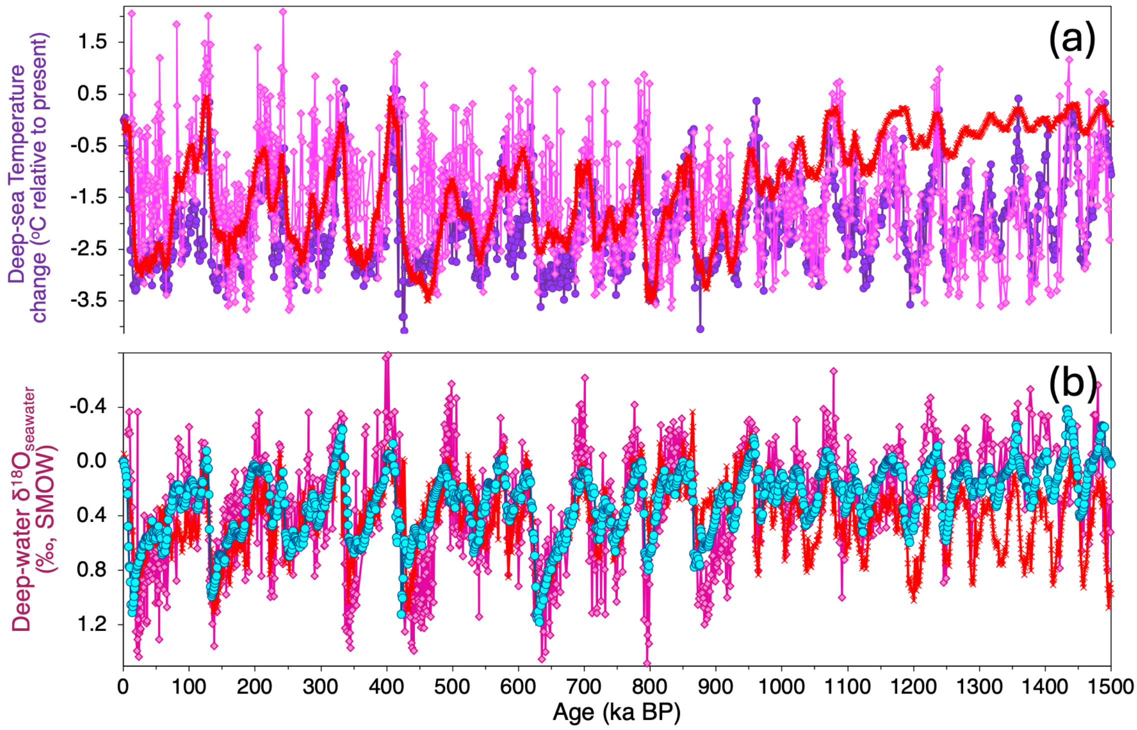

Figure S1: Comparison of deep-water temperature and $\delta^{18}O_{seawater}$ reconstructions derived from proxy- and process-based approaches.
(a) Deep-water temperature reconstructions relative to the present using Mg/Ca-palaeothermometry from Site 1123 (pink line with diamonds; Elderfield et al., 2012) and process-based approaches from Rohling et al. (2021) (purple line and circles) and Clark et al. (2025a) (red line with crosses). (b) $\delta^{18}O_{seawater}$ reconstructions derived using the same approaches in (a) from Site 1123 (dark pink line with diamonds; Elderfield et al., 2012) and process-based reconstructions from Rohling et al. (2021) (blue line and circles) and Clark et al. (2025a) (red line with crosses).

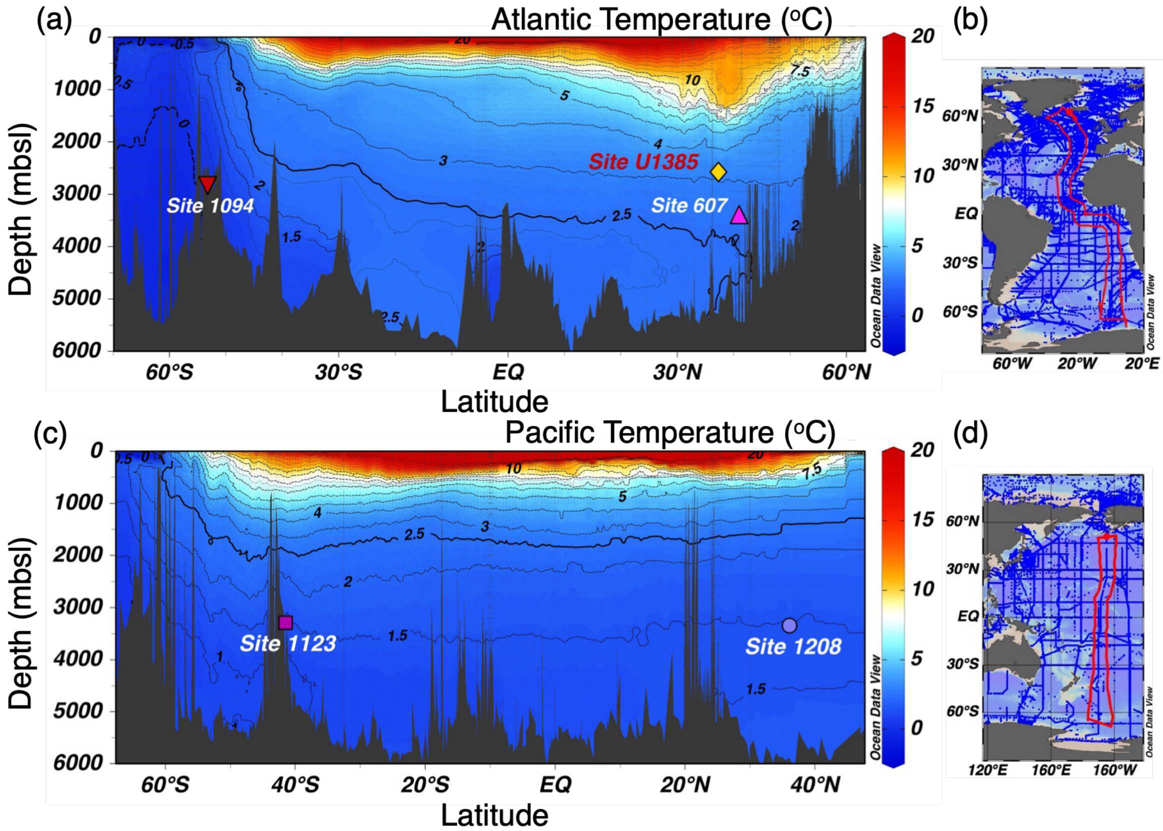

Figure S2: (a) Atlantic and (c) Pacific meridional hydrographic profiles of deep-water temperature (°C) relative to site locations and depths as in Fig. 1. (b) and (d) show the transect routes for the Atlantic and Pacific hydrographic profiles, respectively (red lines). Temperature values are reported as potential temperature (θ), obtained from GLODAPv2.2021 and accessed using Ocean Data View (Schlitzer, 2019; http://odv.awi.de).

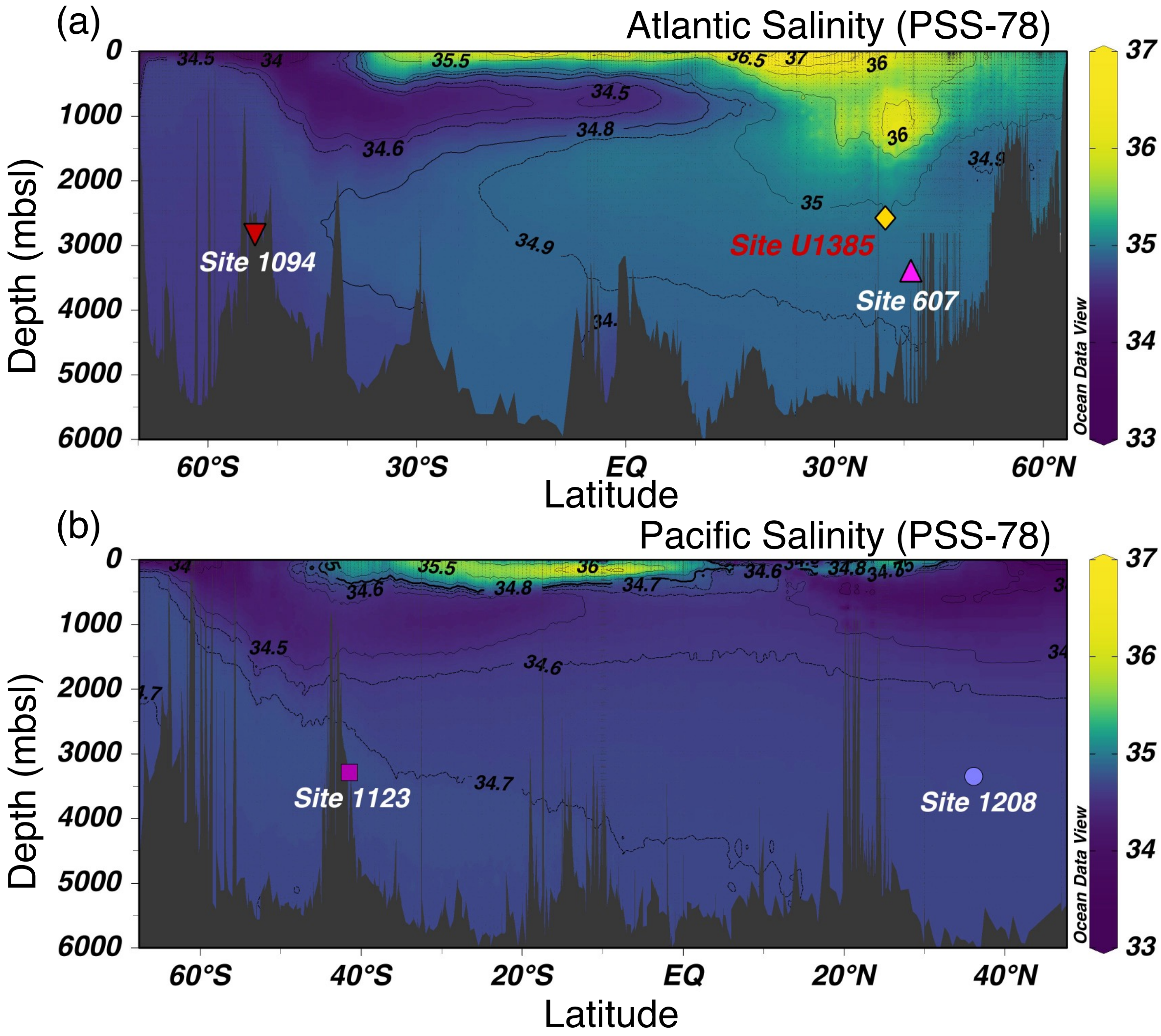

Figure S3: (a) and (b) respectively Atlantic and Pacific Ocean meridional hydrographic profiles of deep-water salinity showing site locations and depths as in Fig. 1. Hydrographic profiles follow the transect routes shown in Fig. S1b, d. Salinity is reported as practical salinity (PSS-78), following the convention of the GLODAPv2 datasets and accessed using Ocean Data View (Schlitzer, 2019; <u>http://odv.awi.de</u>).

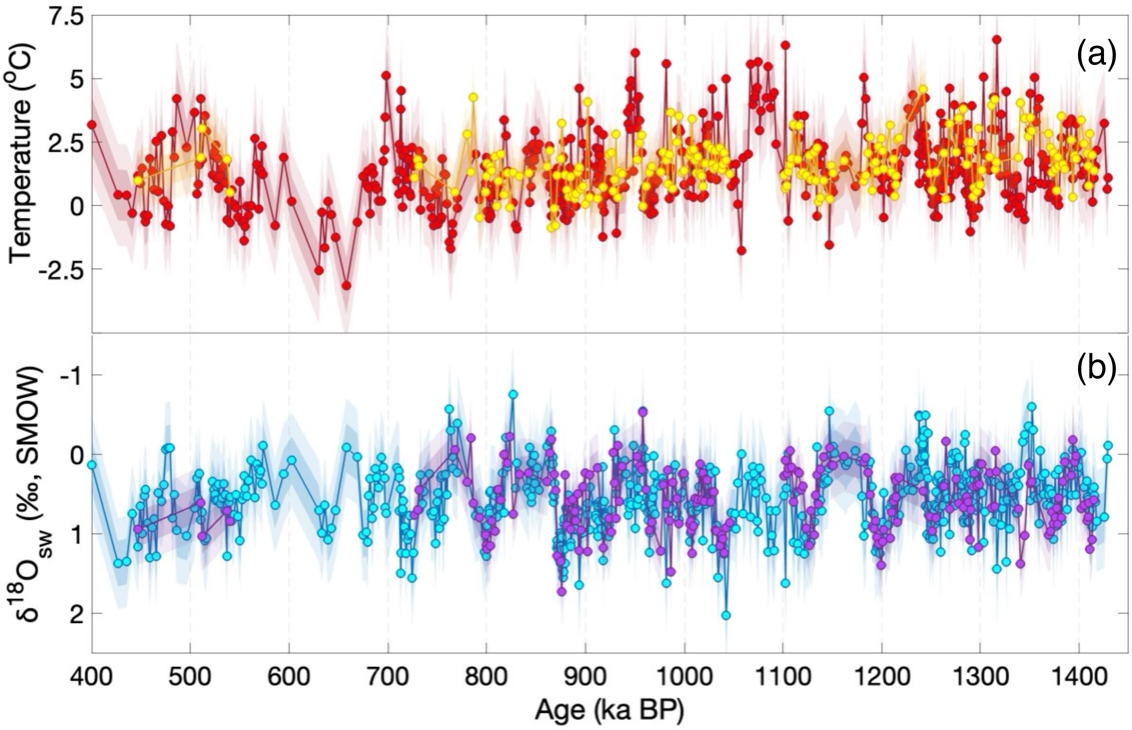

Figure S4: Comparison of deep-water temperature and $\delta^{18}O_{seawater}$ estimates derived from $\delta^{18}O$ and Mg/Ca measurements of *Uvigerina peregrina* and *Globobulimina affinis* at Site U1385. (a) Mg/Ca-derived deep-water temperature for *Uvigerina peregrina* (red) and *Globobulimina affinis* (yellow). (b) Corresponding $\delta^{18}O_{seawater}$ estimates based on *Uvigerina peregrina* (blue) and *Globobulimina affinis* (purple). Uncertainty envelopes (same colours) show 1σ and 2σ ranges (dark and light shading, respectively), incorporating both analytical and calibration uncertainties.

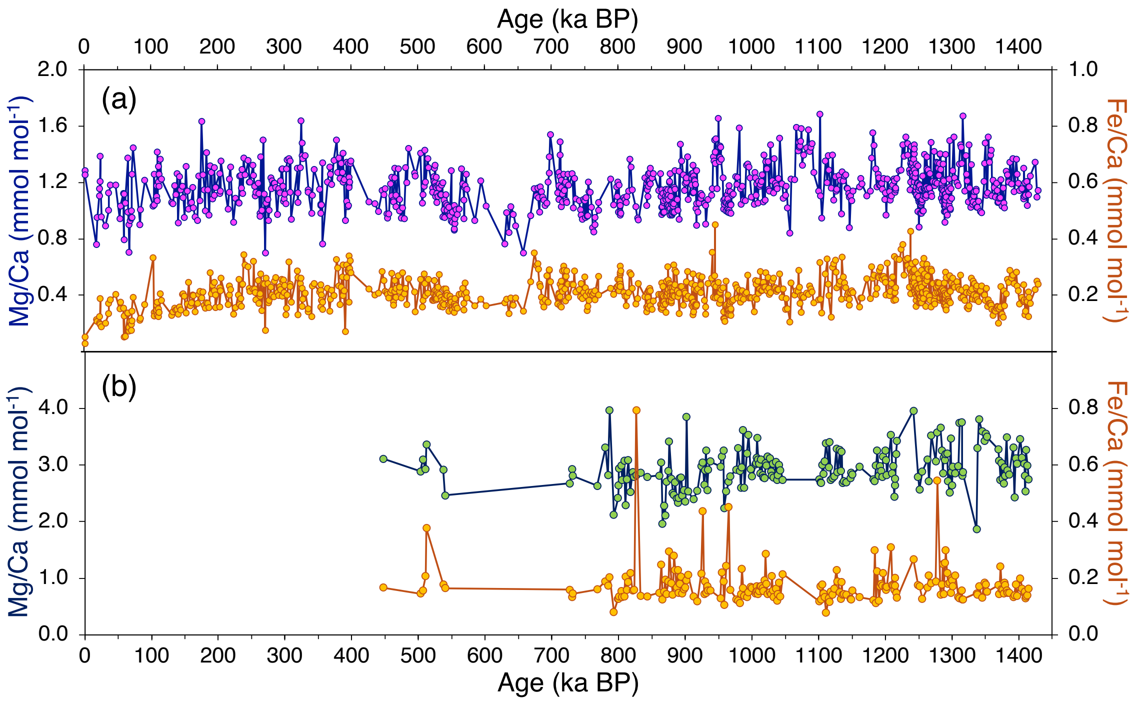

Figure S5: Site U1385 measured Mg/Ca and Fe/Ca after assessment and removal of co-occurring high values. (a) Comparison of *Uvigerina peregrina* Mg/Ca (dark blue line and pink circles) and Fe/Ca (light brown line with yellow circles). (b) Same as in (a) but with measurements made on *Globobulimina affinis* Mg/Ca (dark blue line and green circles) and Fe/Ca (light brown line with yellow circles). Note the larger scale for *G. affinis* Mg/Ca relative to *U. peregrina*.

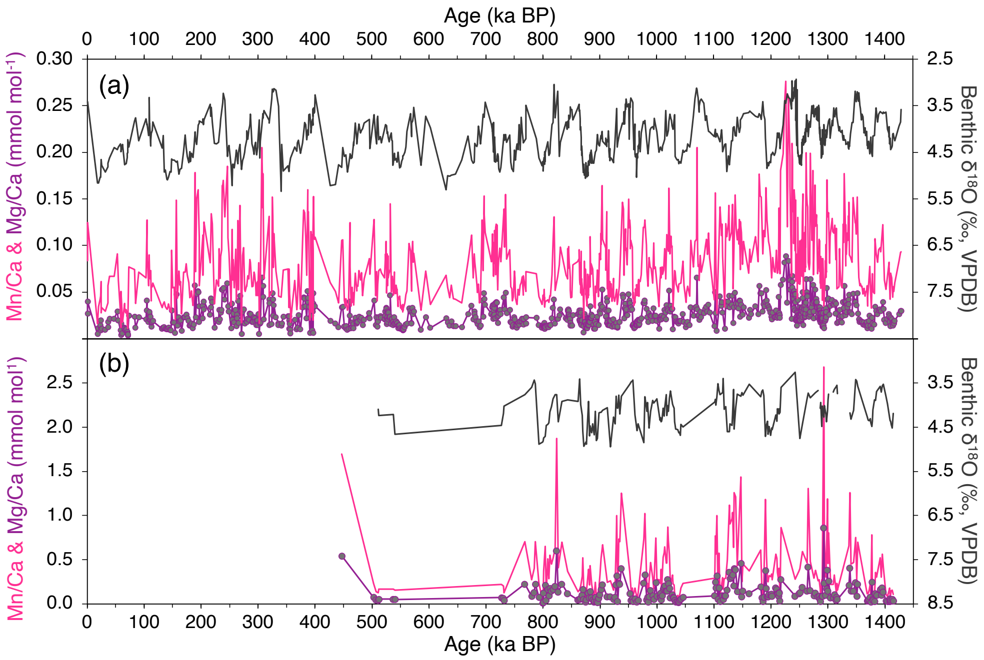

Figure S6: Downcore glacial-interglacial variations in Site U1385 Mn/Ca. (a) Glacial-interglacial variations depicted by benthic $\delta^{18}O$ (black line); Mn/Ca measured on *Uvigerina peregrina* (pink line) which tends to increase downcore and shows greatest values during interglacials and interstadials with minimum values recorded during glacials; and Mg/Ca correction values (purple line with grey circles) calculated from the Mg/Mn coating correction ratio of 0.32 mol mol^{-1} (Hasenfratz et al., 2017; de Lange et al., 1992) discussed in text. (b) Mn/Ca and Mg/Ca as in (a) measured on *Globobulimina affinis*. Note the larger scale relative to (a).

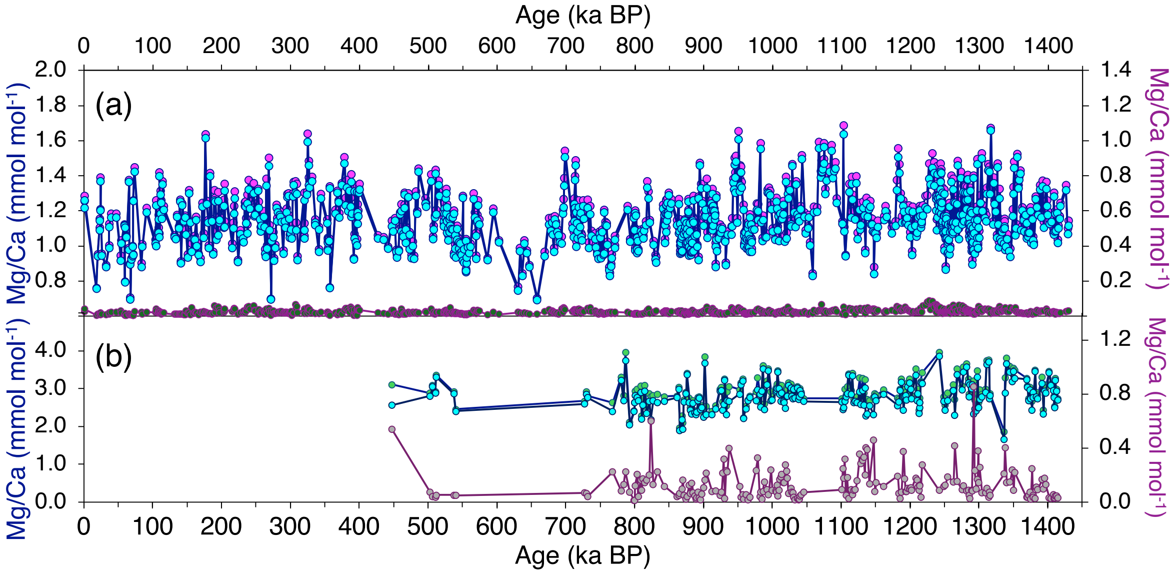

Figure S7: Mg/Ca data after correction for foraminiferal coating Mg/Mn ratios. (a) *Uvigerina peregrina* measured Mg/Ca (dark blue line with pink circles); Mg/Ca corrected by 0.32 mol mol^{-1} (dark blue line light blue circles); and foraminiferal coating corrections calculated from the Mg/Mn ratio of 0.32 mol mol^{-1} (Hasenfratz et al., 2017; de Lange et al., 1992) (plum with grey circles). (b) The same as in (a) but for *Globobulimina affinis* with green circles instead of pink. Note the larger Mg/Ca scale relative to (a).

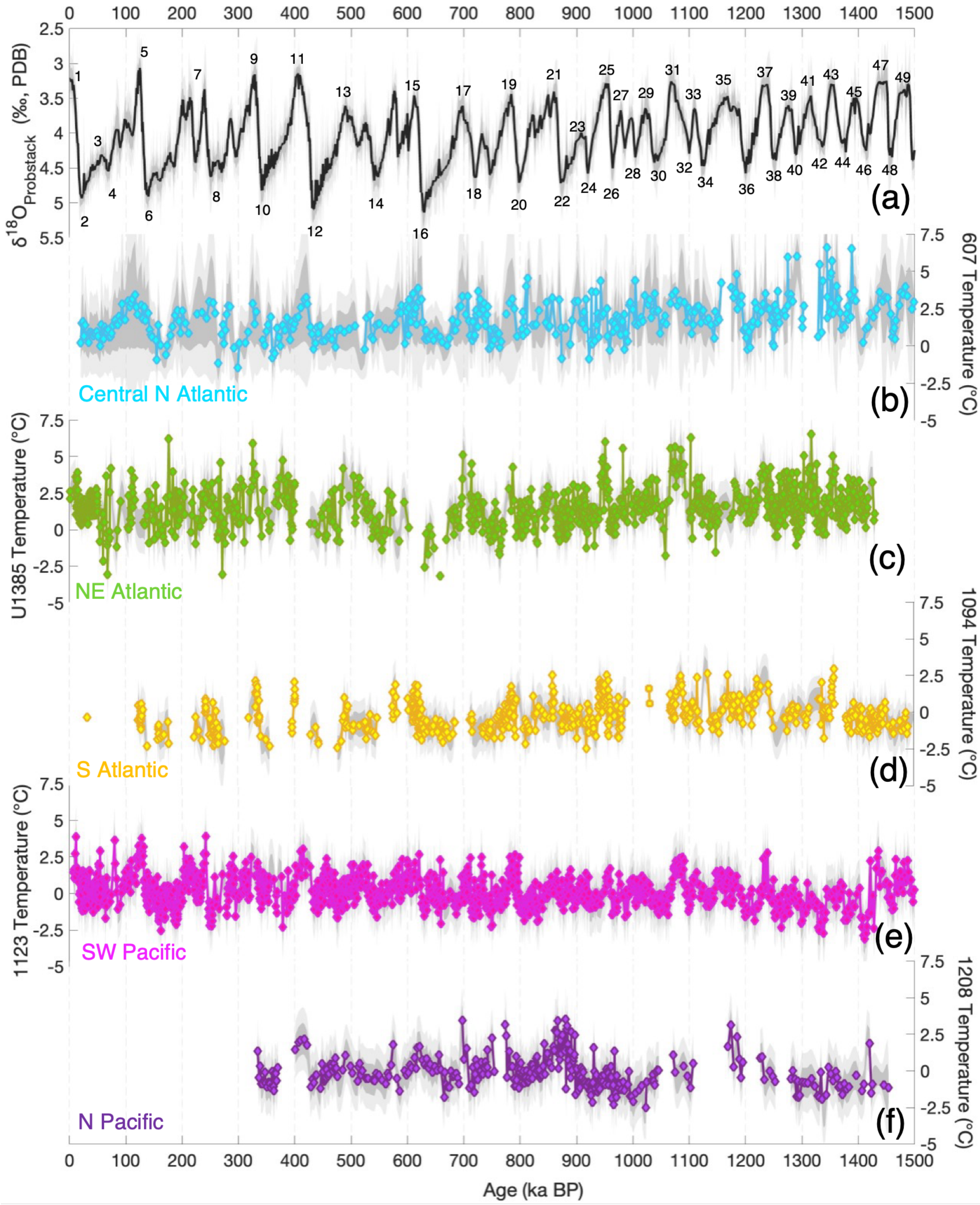

Figure S8: Deep-water Mg/Ca-derived temperature for all sites calculated using PSU Solver (Thirumalai et al., 2016). (a) Prob-stack benthic $\delta^{18}O$ (Ahn et al., 2017) (black line) with MIS numbers denoting glacial (even) and interglacial (odd) stages. (b) DSDP Site 607 (Ford et al., 2016; Sosdian and Rosenthal, 2009) (light blue); (c) IODP Site U1385 (this study, including other Iberian Margin records (Birner et al., 2016; Skinner et al., 2003; Skinner and Elderfield, 2007) (light green); (d) ODP Site 1094 (Hasenfratz et al., 2019) (yellow); (e) ODP Site 1123 (Elderfield et al., 2012) (light pink); and (f) ODP Site 1208 (Ford and Raymo, 2020) (dark purple). Shading represents 1 and 2σ error envelopes propagated from analytical and calibration sources (dark and light grey respectively).

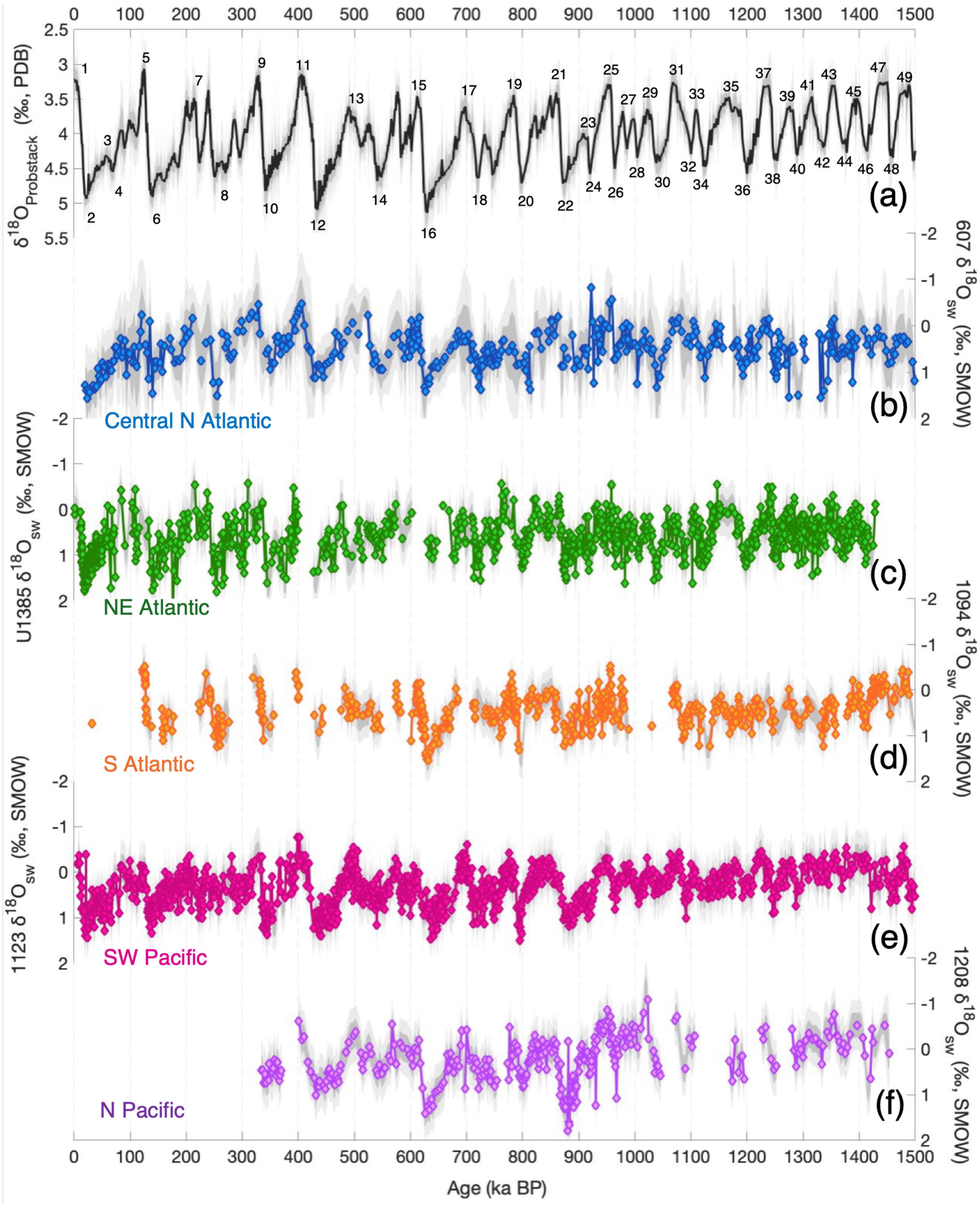

Figure S9: $\delta^{18}O_{seawater}$ for all sites calculated using PSU Solver (Thirumalai et al., 2016). (a) Probstack benthic $\delta^{18}O$ (Ahn et al., 2017) (black line) with MIS numbers denoting glacial (even) and interglacial (odd) stages. b) DSDP Site 607 (Ford et al., 2016; Sosdian and Rosenthal, 2009) (blue); (c) IODP Site U1385 (this study, including other Iberian Margin records (Birner et al., 2016; Skinner et al., 2003; Skinner and Elderfield, 2007) (green); (d) ODP Site 1094 (Hasenfratz et al., 2019) (orange); (e) ODP Site 1123 (Elderfield et al., 2012) (pink and (f) ODP Site 1208 (Ford and Raymo, 2020) (purple). Dark and light grey shading represents 1 and 2σ error bars respectively propagated from analytical and calibration uncertainties.

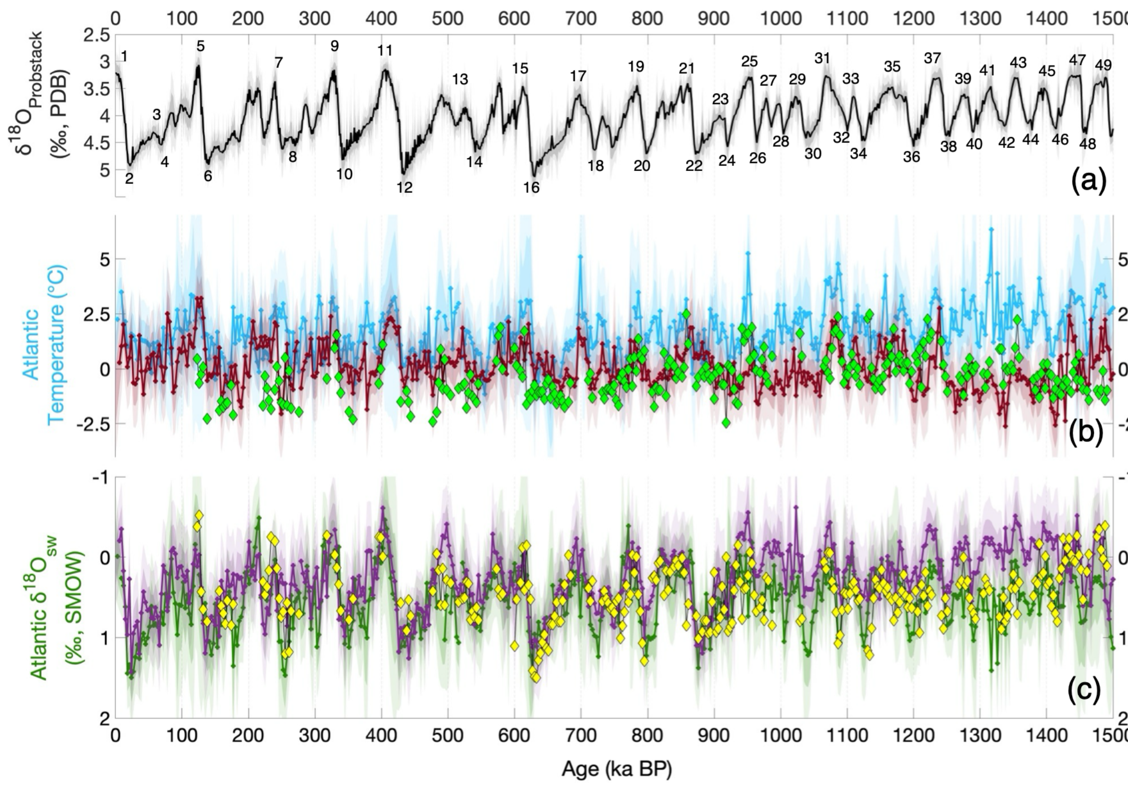

Figure S10: Comparison of Site 1094 (South Atlantic sector of Southern Ocean) with North Atlantic and Pacific Ocean temperature and benthic $\delta^{18}O_{seawater}$ stacks. (a) Prob-stack benthic $\delta^{18}O$ (Ahn et al., 2017) (black line), with MIS numbers denoting glacial stages (below) and interglacials (above). (b) Deep-water temperature stacks for the Pacific Ocean (Elderfield et al., 2012; Ford and Raymo, 2020) (dark red), and the North Atlantic Ocean (this study and (Ford et al., 2016; Sosdian and Rosenthal, 2009) (light blue), overlain by Site 1094 deep-water temperature (Hasenfratz et al., 2019) (green diamonds). (c) Deep-water $\delta^{18}O_{seawater}$ stacks for the Pacific Ocean (Elderfield et al., 2012; Ford and Raymo, 2020) (purple) and the North Atlantic (this study including (Ford et al., 2016; Sosdian and Rosenthal, 2009)) (green), overlain by Site 1094 deep-water $\delta^{18}O_{seawater}$ (Hasenfratz et al., 2019) (yellow diamonds). Stacks and their error envelopes represent the mean of interpolated (on 3 kyr interval) and bootstrapped records with uncertainties reflecting both analytical error and the spread between paired estimates (see Sect. 2.6).

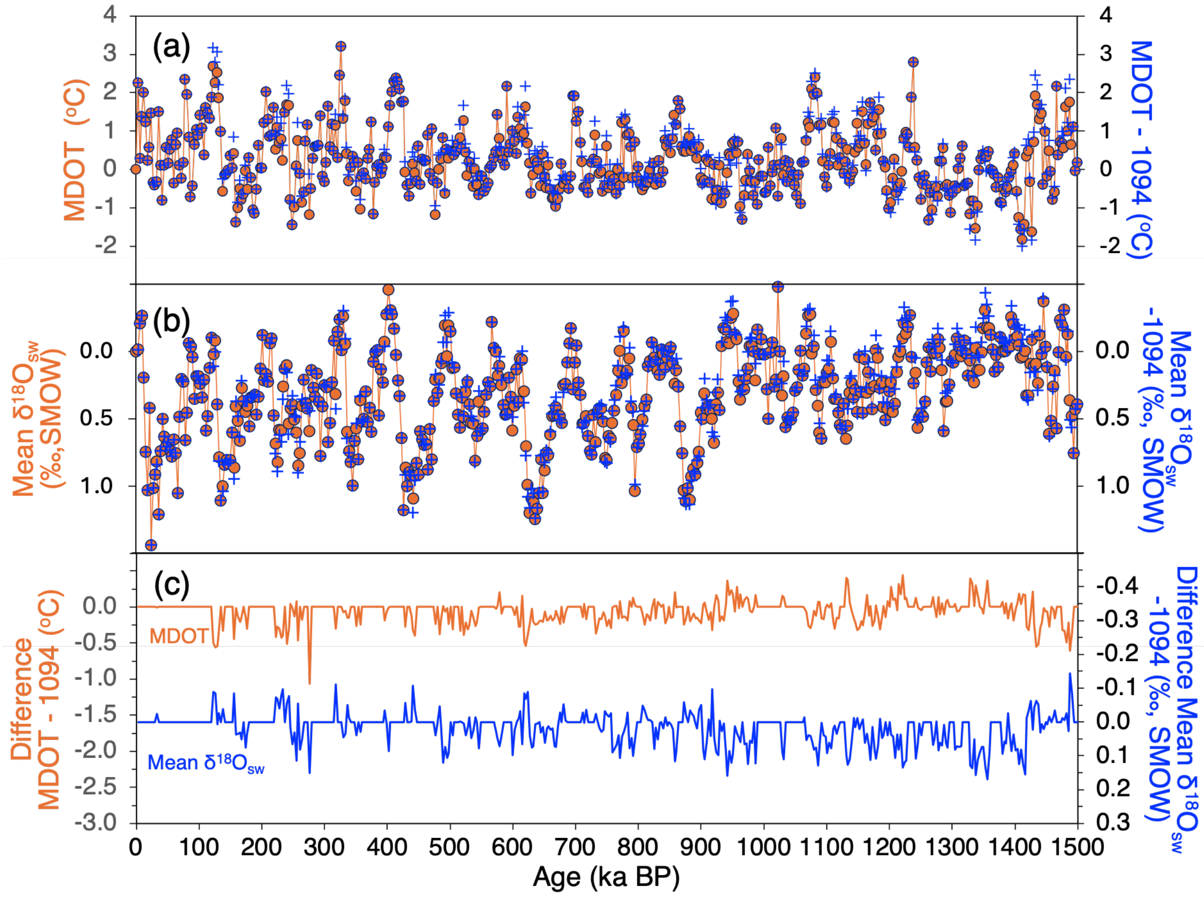

Figure S11: Sensitivity of stacked records to the inclusion of South Atlantic Site 1094. Upper panels show the basin volume–weighted stacks of MDOT (a) and mean $\delta^{18}O_{seawater}$ (b), calculated using the full dataset (filled orange circles) and excluding Site 1094 (Hasenfratz *et al.*, 2019) (blue crosses). The close agreement between the two reconstructions indicates minimal visual differences in the structure, amplitude, and timing of the records.
Lower panel (c) shows the differences between the full stacks and those calculated without Site 1094, with MDOT shown in orange and $\delta^{18}O_{seawater}$ in blue. Differences are small, centred around zero, and lack any distinct trends, demonstrating that data gaps in the South Atlantic exert minimal influence on the globally stacked records.

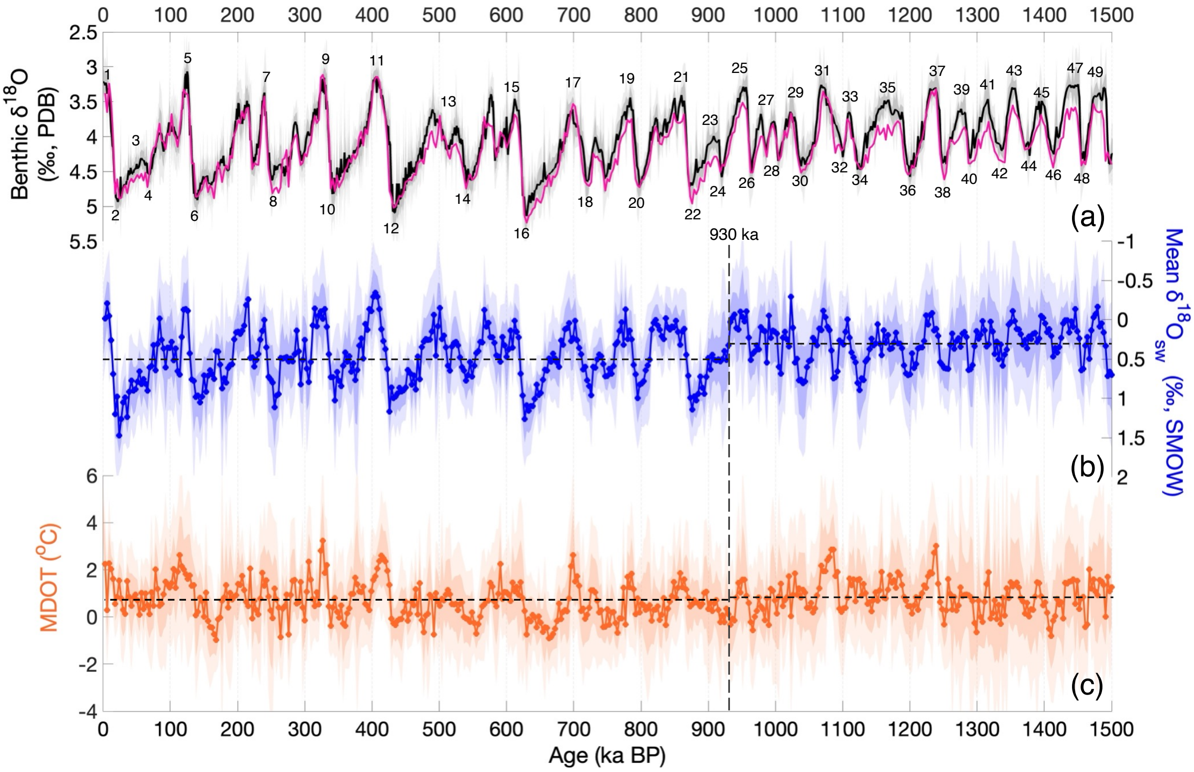

Figure S12: Non-weighted mean ocean stacks. (a) Benthic $\delta^{18}O$ (pink), (b) Mean deep-water $\delta^{18}O_{seawater}$ (blue) and (c) MDOT (orange). The black curve in (a) shows the Prob-stack benthic $\delta^{18}O$ (Ahn et al., 2017); MIS numbers denote glacial (even) and interglacial (odd) stages. The vertical dashed line marks 930 ka. Horizontal dashed lines in b and c indicate the mean values for the intervals before and after 930 ka. Stacks and their associated uncertainties represent the mean of manually aligned, interpolated (3 kyr resolution) and bootstrapped records, with uncertainties reflecting both analytical error and the spread between paired estimates (see Sect. 2.6).

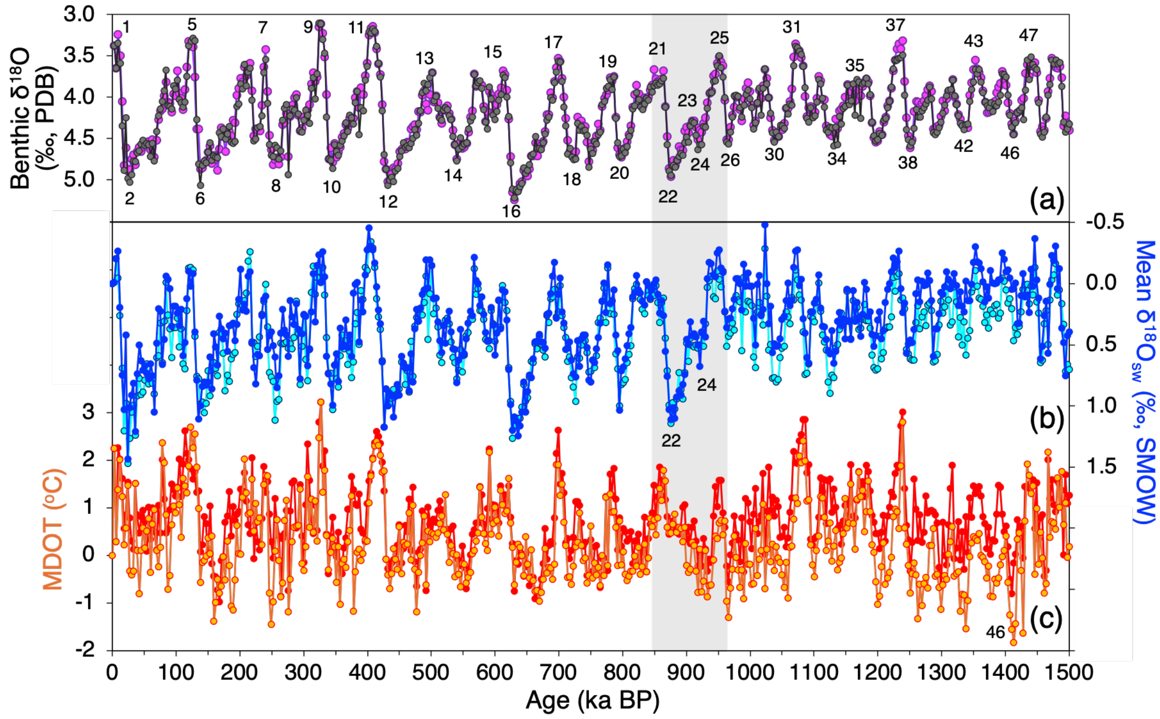

Figure S13: Comparison of unweighted and volume-weighted mean deep ocean stacks. (a) Unweighted (pink) and weighted (dark grey) benthic δ^{18}O with MIS numbers highlighting selected glacial (even) and interglacial (odd) stages. (b) Comparisons for globally distributed mean δ^{18}O$_{seawater}$ between unweighted (light blue) versus volume-weighted (dark blue) stacks; and (c) comparisons for MDOT between the unweighted (red) and volume-weighted (orange) stacks with the latter suggesting MIS 46 (~1420 ka) experienced the coldest deep-water temperatures of the last 1.5 Ma.

Table S1: Ocean basin boundaries and volumes

Region	Depth Range	Latitude Range	Longitude Range	Volume (% global ocean)*
Deep North Atlantic	2000–5000 m	0–65°N	80°W-0°	5.1
Deep South Atlantic	2000–5000 m	70°S–0	70°W-30°E	7
Deep Pacific Ocean	2000–5000 m	70°S–55°N	105°E-70°W	31.5
Total global ocean represented				43.6

*Note: to construct global weighted stacks, the percent volume for each basin is scaled to the sum of the regional volumes (i.e. 43.6 % when all three basins are represented). For example, the relative volume of the deep North Atlantic in this case is 5.1 / 43.6 = 11.7 %. In some cases, the entire value from a single basin is represented (Atlantic n = 2; Pacific n = 4). After Lisiecki and Stern (2016).

References

Ahn, S., Khider, D., Lisiecki, L. E., and Lawrence, C. E.: A probabilistic Pliocene–Pleistocene stack of benthic $\delta^{18}O$ using a profile hidden Markov model, Dyn. Stat. Clim. Syst., 2, 1–16, https://doi.org/10.1093/climsys/dzx002, 2017.

Birner, B., Hodell, D. A., Tzedakis, P. C., and Skinner, L. C.: Similar millennial climate variability on the Iberian Margin during two early Pleistocene glacials and MIS 3, Paleoceanography, 31, 203–217, https://doi.org/10.1002/2015PA002868, 2016.

Clark, P. U., Shakun, J. D., Rosenthal, Y., Zhu, C., Bartlein, P. J., Gregory, J. M., Köhler, P., Liu, Z., and Schrag, D. P.: Mean ocean temperature change and decomposition of the benthic $\delta^{18}O$ record over the past 4.5 million years, Clim. Past, 21, 973–1000, 2025a.

Elderfield, H., Yu, J., Anand, P., Kiefer, T., and Nyland, B.: Calibrations for benthic foraminiferal Mg/Ca paleothermometry and the carbonate ion hypothesis, Earth Planet. Sci. Lett., 250, 633–649, https://doi.org/10.1016/j.epsl.2006.07.041, 2006.

Elderfield, H., Greaves, M., Barker, S., Hall, I. R., Tripati, A., Ferretti, P., Crowhurst, S., Booth, L., and Daunt, C.: A record of bottom water temperature and seawater $\delta^{18}O$ for the Southern Ocean over the past 440 kyr based on Mg/Ca of benthic foraminiferal *Uvigerina* spp., Quat. Sci. Rev., 29, 160–169, https://doi.org/10.1016/j.quascirev.2009.07.013, 2010.

Elderfield, H., Ferretti, P., Greaves, M., Crowhurst, S. J., McCave, I. N., Hodell, D., and Piotrowski, A. M.: Evolution of ocean temperature and ice volume through the Mid-Pleistocene Climate Transition, Science, 337, 704–709, https://doi.org/10.1126/science.1221294, 2012.

Ford, H. L. and Raymo, M. E.: Regional and global signals in seawater $\delta^{18}O$ records across the mid-Pleistocene transition, Geology, 48, 113–117, https://doi.org/10.1130/G46546.1, 2020.

Ford, H. L., Sosdian, S. M., Rosenthal, Y., and Raymo, M. E.: Gradual and abrupt changes during the Mid-Pleistocene Transition, Quat. Sci. Rev., 148, 222–233, https://doi.org/10.1016/j.quascirev.2016.07.005, 2016.

Greaves, M. J.,: Trace Elements in Marine Biogenic Carbonates: Analysis and Application to Past Ocean Chemistry, Ph.D. thesis, University of Southampton 194 pp., https://eprints.soton.ac.uk/63291/, 2008.

Hasenfratz, A. P., Martínez-García, A., Jaccard, S. L., Vance, D., Wälle, M., Greaves, M., and Haug, G. H.: Determination of the Mg/Mn ratio in foraminiferal coatings: An approach to correct Mg/Ca temperatures for Mn-rich contaminant phases, Earth Planet. Sci. Lett., 457, 335–347, https://doi.org/10.1016/j.epsl.2016.10.004, 2017.

Hasenfratz, A. P., Jaccard, S. L., Martínez-García, A., Sigman, D. M., Hodell, D. A., Vance, D., Bernasconi, S. M., Kleiven, H. (Kikki) F., Haumann, F. A., and Haug, G. H.: The residence time of Southern Ocean surface waters and the 100,000-year ice age cycle, Science, 363, 1080–1084, https://doi.org/10.1126/science.aat7067, 2019.

de Lange, G. J., van Os, B., and Poorter, R.: Geochemical composition and inferred accretion rates of sediments and managanese nodules from a submarine hill in the Madeira Abyssal Plain, eastern North Atlantic, Mar. Geol., 109, 171–194, https://doi.org/10.1016/0025-3227(92)90227-9, 1992.

Lisiecki, L. E. and Stern, J. V.: Regional and global benthic $\delta^{18}O$ stacks for the last glacial cycle, Paleoceanography, 31, 1368–1394, https://doi.org/10.1002/2016PA003002, 2016.

Martin, W. R. and Sayles, F. L.: $CaCO_3$ dissolution in sediments of the Ceara Rise, western equatorial Atlantic, Geochim. Cosmochim. Acta, 60, 243–263, https://doi.org/10.1016/0016-7037(95)00383-5, 1996.

Mashiotta, T. A., Lea, D. W., and Spero, H. J.: Glacial-interglacial changes in Subantarctic sea surface temperature and $\delta^{18}O$-water using foraminiferal Mg, Earth Planet. Sci. Lett., 170, 417–432, https://doi.org/10.1016/S0012-821X(99)00116-8, 1999.

Rohling, E. J., Yu, J., Heslop, D., Foster, G. L., Opdyke, B., and Roberts, A. P.: Sea level and deep-sea temperature reconstructions suggest quasi-stable states and critical transitions over the past 40 million years, Sci. Adv., 7, 1–7, https://doi.org/10.1126/sciadv.abf5326, 2021.

Skinner, L. C. and Elderfield, H.: Rapid fluctuations in the deep North Atlantic heat budget during the last glacial period, Paleoceanography, 22, PA1205, https://doi.org/10.1029/2006PA001338, 2007.

Skinner, L. C., Shackleton, N. J., and Elderfield, H.: Millennial-scale variability of deep-water temperature and $\delta^{18}O_{dw}$ indicating deep-water source variations in the Northeast Atlantic, 0-34 cal. ka BP, Geochem, Geophys. Geosyst., 4, 1098, https://doi.org/10.1029/2003GC000585, 2003.

Sosdian, S. and Rosenthal, Y.: Deep-sea temperature and ice volume changes across the Pliocene-Pleistocene climate transitions, Science, 325, 306–310, https://doi.org/10.1126/science.1169938, 2009.

Stirpe, C. R., Allen, K. A., Sikes, E. L., Zhou, X., Rosenthal, Y., Cruz-Uribe, A. M., and Brooks, H. L.: The Mg/Ca proxy for temperature: A Uvigerina core-top study in the Southwest Pacific, Geochim. Cosmochim. Acta, 309, 299–312, https://doi.org/10.1016/j.gca.2021.06.015, 2021.

Thirumalai, K., Quinn, T. M., and Marino, G.: Constraining past seawater $\delta^{18}O$ and temperature records developed from foraminiferal geochemistry, Paleoceanography, 31, 1409–1422, https://doi.org/10.1002/2016PA002970, 2016.

Weldeab, S., Arce, A., and Kasten, S.: Mg/Ca-$\Delta CO^{2-}_{3 \text{pore water}}$-temperature calibration for *Globobulimina* spp.: A sensitive paleothermometer for deep-sea temperature reconstruction, Earth Planet. Sci. Lett., 438, 95–102, https://doi.org/10.1016/j.epsl.2016.01.009, 2016.

Yu, J. and Broecker, W. S.: Comment on "Deep-sea temperature and ice volume changes across the Pliocene-Pleistocene Climate Transitions," Science, 328, 1480, https://doi.org/10.1126/science.1186544, 2010.

Yu, J. and Elderfield, H.: Mg/Ca in the benthic foraminifera Cibicidoides wuellerstorfi and Cibicidoides mundulus: Temperature versus carbonate ion saturation, Earth Planet. Sci. Lett., 276, 129–139, https://doi.org/10.1016/j.epsl.2008.09.015, 2008.